Journal of Fluorine Chemistry 198 (2017) 54–60

Contents lists available at ScienceDirect

Journal of Fluorine Chemistry

journal homepage: www.elsevier.com/locate/fluor

Full Length Article

Structural characterization of new fluorinated mesogens obtained through halogen-bond driven self-assembly

Vijith Kumar[a], Dirk J. Mulder[b,c], Gabriella Cavallo[a,*], Tullio Pilati[a], Giancarlo Terraneo[a], Giuseppe Resnati[a], Albertus P.H.J. Schenning[b,d], Pierangelo Metrangolo[a,e]

[a] NFMLab - D.C.M.I.C. "Giulio Natta", Politecnico di Milano, Via L. Mancinelli 7, 20131 Milan, Italy
[b] Department of Functional Organic Materials and Devices, Chemical Engineering and Chemistry, Eindhoven University of Technology, Den Dolech 2, 5612 AZ, Eindhoven, The Netherlands
[c] Dutch Polymer Institute (DPI), PO Box 902, 5600 AZ, Eindhoven, The Netherlands
[d] Institute for Complex Molecular Systems (ICMS), Eindhoven University of Technology, P.O. Box 513, 5600 MB, Eindhoven, The Netherlands
[e] VTT-Technical Research Centre of Finland, P.O. Box 1000, FI-02044 VTT, Finland

ARTICLE INFO

Article history:
Received 26 October 2016
Received in revised form 6 December 2016
Accepted 9 December 2016
Available online 3 January 2017

Keywords:
Self-assembly
Halogen bonding
Liquid crystals
Reactive mesogens
Diiodoperfluorocarbons

ABSTRACT

We describe the synthesis and characterization of new trimeric complexes obtained upon halogen-bond driven self-assembly of 1,4-diiodotetrafluorobenzene or α,ω– diiodoperfluoroalkanes, acting as XB-donors, with an alkoxystilbazole derivative functionalized with a methacrylate terminal group, acting as XB-acceptor. Despite the fact that the starting materials are not mesomorphic in nature, the obtained halogen-bonded complexes exhibit monotropic LC behaviour with smectic A phases possibly resulting from segregation between fluorocarbon and hydrocarbon chains. The obtained supramolecular mesogens possess reactive groups suitable for incorporation into liquid crystalline elastomeric actuators.

1. Introduction

Composed of anisotropic organic molecules, liquid crystals (LCs) are fluids exhibiting a long range order and for this reason they are often referred to as the fourth state of the matter, in between the solid and the liquid phases [1]. Since their discovery in the late 19th century, liquid crystals have had a profound impact on modern technology [2]. Their application in flat panel displays has paved the way to the design of a number of new electronic devices. Their exotic and unique behaviour still continues to fascinate academic and industrial researchers around the world, with actual and postulated applications well beyond the realm of flat panel displays [3].

In recent years the self-assembly of LCs has been successfully exploited for the development of new functional nanostructured organic materials. [4,5] In such materials a well-defined hierarchical order is crucial in order to generate the desired functional properties, and the *in situ* polymerization of reactive liquid crystal monomers, in the molten phase, represents a fast and controllable process for the production of stable anisotropic polymers and networks [6]. Monomers containing reactive end groups such as acrylate, diene or diacetylene moiety are first aligned macroscopically in the liquid crystalline phase, then the alignment can be frozen by *in situ* polymerization induced either thermally or under UV irradiation, affording to nanostructured polymers characterized by a stable LC order over a wide temperature range.

Functional organic materials based on polymerised LC assemblies have been largely investigated for applications as membranes [7], drug delivery systems [3] optically anisotropic films [8], holographic materials [9], soft stimuli-responsive actuators [10,11] and sensors [12]. The macroscopic properties and phase structures of the resulting polymeric LC systems, and consequently their final application, are strictly related to the cross-linking density of the final network. For example, stimuli-responsive soft actuators, for application as artificial muscles, can be realized by weakly cross-linking the starting reactive mesogens [13]. The product is a liquid crystalline elastomer, where the anisotropy of the LCs and the elasticity of a rubber are combined in order to obtain actuating ability. In order to produce functional organic materials with new properties and enhanced responses, there is a need to extend the toolbox of available reactive mesogens and combine different triggers in LC materials.

* Corresponding author.
E-mail address: gabriella.cavallo@polimi.it (G. Cavallo).

http://dx.doi.org/10.1016/j.jfluchem.2016.12.011

As a complement of hydrogen bonding (HB), halogen bonding (XB) is emerging as a noncovalent interaction of choice in designing functional supramolecular materials [14]. According to IUPAC, the term halogen bonding refers to the noncovalent attractive interaction involving a halogen atom as the electrophilic site [15]. XB is a highly directional interaction, whose strength can be easily tuned by changing the halogen atom (XB-donor) and the electron-withdrawing ability of the substituents in its neighbourhood [16,17]. The strength of the XB, in fact, increases with the polarizability of the halogen atom, while the presence of electron withdrawing substituents at the vicinity of the XB-donor site increases its Lewis acidity and consequently the interaction strength. In particular fluorination of the molecular backbone of certain halogenated building blocks enhances their ability to work as XB-donors, giving rise to particularly strong interactions [18]. The electron-donating XB-acceptors can be either anions or neutral species possessing at least one nucleophilic region, e.g., a lone-pair-possessing heteroatom or a π-system.

Thanks to its high directionality, the XB has been applied successfully in the construction of new liquid crystalline materials [19,20]. Moreover, its high specificity for haloperfluorocarbons allowed the introduction of fluorinated modules [21–23], overcoming the low affinity existing between perfluorocarbon and hydrocarbon compounds and opening new opportunities for exerting control over the mesomorphic phase and the functional properties of the final systems. Fluorination, in fact, represents an efficient strategy to enhance physical properties and to exert control over the supramolecular organization in liquid crystals [24,25]. Generally, the introduction of perfluorinated chains results in higher transition temperatures while the well-known tendency of perfluoroalkyl chains to segregate from hydrocarbon chains favours the formation of lamellar phases. This produces interesting charge-transport properties in ionic liquid crystals where anisotropic conduction pathways can be generated [26,27].

Some years ago, our group has reported about the liquid crystalline behaviour of halogen-bonded trimeric complexes obtained upon self-assembly of a range of alkoxystilbazoles acting as monodentate XB-acceptors with α,ω;-diiodoperfluoroalkanes or 1,4-diiodotetrafluorobenzene acting as bidentate XB-donors [23,28]. Despite the non-mesomorphic nature of the starting materials, most of the reported halogen-bonded complexes have shown liquid-crystallinity. The modularity of this approach has opened new perspectives in the engineering of liquid crystals and, liquid crystalline polymers with nematic phases have been obtained upon complexation of difunctional XB-donor and acceptor molecules [29], while reacting an alkoxystilbazole derivative with a XB-donor molecule incorporating an azo group, supramolecular LC complexes with unique light-responsive properties have been obtained [30].

Keen to explore the potential of XB in the formation of new reactive mesogens, on the heels of our previous results, we have prepared some new halogen bonded complexes by self-assembly of 1,4-diiodotetrafluorobenzene and α,ω–diiodoperfluoroalkanes of different chain length, with an alkoxystilbazole derivative bearing an alkoxy chain functionalized with a terminal methacrylate group (Scheme 1). The formation, the structural characterization, and the mesomorphic behaviour of such materials are herein described in detail.

2. Results and discussion

2.1. Synthesis of supramolecular complexes

Diiodoperfluoroalkanes and diiodoperfluoroarenes are well-known XB donors, largely applied for the construction of numerous supramolecular structures [31–34] and liquid crystals [20], since they form particularly short and directional interactions, thus allowing structural control over the final supramolecular complexes. From their bifunctional structures it may be expected that trimeric complexes where the fluorinated module is bridging two stilbazole derivatives **1** are obtained. Therefore, the XB-complexes **3a**–**e** between the stilbazole methacrylate **1** and the diiodoperfluorocarbons **2a**–**e** (Scheme 1) have been obtained by crystallizing from THF solutions a 2:1 mixture of the stilbazole methacrylate and the diiodoperfluorocarbon. The successful complex formation was soon evidenced by a color change in the products. In fact both the parent stilbazole methacrylate and the diiodoperfluorocarbons are white, whereas crystals obtained from THF solutions were pale yellow implying a degree of charge transfer from the pyridine nitrogen to the σ-hole on the iodine atom [35].

All the complexes were characterized by FTIR spectroscopy, single crystal X-ray diffraction analysis, and Polarized Optical Microscopy (POM).

2.2. FTIR spectroscopy

Fourier transform infrared spectroscopy (FTIR) has been applied as a simple and fast screening method to detect the occurrence of XB between the stilbazole derivative **1** and the diiodoperfluorocarbons **2**. It is well-known, in fact, that the intermolecular interaction between an electron-donor species with an electrophile affects the vibrational motions in term of intensity and shift.

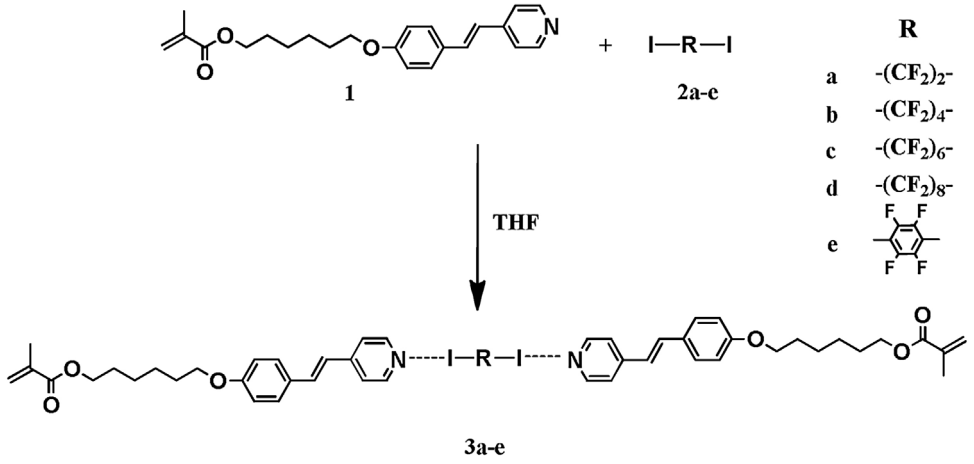

Scheme 1. Chemical structures of the alkoxystilbazole derivative (**1**), the diiodoperfluorocarbon modules (**2a–e**) and their halogen-bonded complexes (**3a–e**).

Table 1
FTIR frequency changes of the XB-acceptor (**1**) and XB-donors (**2a–e**) before and after complexation.

Sample	Pyridine ν_{C-H} stretching	Fluoroalkyl/phenyl ν_{C-F} stretching		Fluoroalkyl/phenyl δ_{C-F} bending
1	3036			
2a		1147	1096	833
3a	3040	1123	1086	826
2b		1192	1129	834
3b	3054	1175	1123	831
2c		1141	1087	833
3c	n.d.[a]	1115	1058	832
2d		1145	1112	838
3d	3037	–	1103	832
2e		1459		940
3e	3044	1456		934

[a] Upon halogen bonding the intensity of the C—H stretching vibration of pyridine ring undergoes a marked reduction and the band is not visible anymore in the spectrum of **3c**.

In pyridine-iodoperfluorocarbon complexes it has been found that the occurrence of halogen-bonding produces a blue-shift and intensity decrease in the pyridine bands in the region 3000–3100 cm^{-1}, as a result of a higher positive charge on the pyridyl hydrogens in the complex, and a red-shift of the bands associated with the perfluorinated moiety, due to an increased electron density of the XB-donor [36,37]. This is clearly evident in the FTIR spectra of all the complexes described in this paper. For instance, the ν_{C-H} absorption of the pyridine ring in the pure stilbazole methacrylate **1** at 3036 cm^{-1} becomes less intense in **3b** and is shifted to 3054 cm^{-1}, while vibrations related to diiodoperfluorobutane at 1192 cm^{-1}, 1129 cm^{-1}, and 834 cm^{-1} are red-shifted at 1175 cm^{-1}, 1123 cm^{-1}, and 831 cm^{-1} respectively upon complexation. Similarly in complex **3e** the ν_{C-H} absorption of the pyridine ring is blue-shifted at 3044 cm^{-1} while the vibrations related to the fluorophenyl moiety at 1459 and 940 cm^{-1} for the diiodotetrafluorobenzene **3e** are red-shifted to 1456 and 936 cm^{-1}, respectively, on complexation. Selected FTIR absorption frequencies for all the complexes **3a**–**3e** and their individual starting components are reported in Table 1.

2.3. Single crystal structural analysis

Single crystals of complexes **3a–e** were grown by slow evaporation of a THF solution containing a 2:1 mixture of the stilbazole methacrylate **1** and the diiodoperfluorocarbons **2a–e**. After a period ranging from 3 to 7 days at room temperature, plate like single crystals suitable for X-ray diffraction analysis were obtained. Detailed crystallographic data for all structures are summarized in Table 2. CCDC no.s 1511609, 1511611, 1511610, 1511612, 1511613 contain the supplementary crystallographic data for complexes **3a–e**.

Single crystal X-ray diffraction analysis of complexes **3a–e** confirmed that in the final cocrystals the stilbazole methacrylate **1** and the diiodoperfluorocarbon modules **2a–e** are present in a 2:1 ratio and I···N XBs are largely responsible for the self-assembly of the complementary modules **1** and **2**. The topology of the primary network is a nice example of the paradigm of the expansion of a ditopic starting module by a linear linker moiety: Each diiodoperfluorocarbon module **2** acts as a linear and ditopic XB-donor while the stilbazole methacrylate derivative **1** behaves as a strong XB-acceptor (Fig. 1). The geometrical parameters describing the XB contacts are reported in Table 3. All the XBs are quite short and linear with values similar to those reported for other halogen bonded systems involving stilbazoles derivatives [21,28]. These features confirm, once again, that the supramolecular synthon I···N is strong and reliable and that the stilbazole core on the XB acceptor module **1** is a very efficient building unit to promote the formation of halogen-bonded adducts.

From the crystal packing point of view it is interesting to note that although the XB donors used in the co-crystal formation are quite diverse either in structure and dimension, four perfluoroalkanes with different alkyl chain lengths and one aromatic unit respectively, the overall packing of the adducts **3a–e** shares strong similarities.

Table 2
Crystallographic data for co-crystals **3a-e**.

Name	3a	3b	3c	3d	3e
Chemical formula	$C_{48}H_{54}N_2O_6F_4I_2$	$C_{50}H_{54}N_2O_6F_8I_2$	$C_{104}H_{108}N_4O_{12}F_{24}I_4$	$C_{108}H_{108}N_4O_{12}F_{32}I_4$	$C_{104}H_{108}N_4O_{12}F_8I_4$
Molecular weight	1084.8	1184.8	1284.8	1384.8	1140.0
Crystal system, space group	Triclinic, P −1	Triclinic, P −1	Triclinic, P −1	Triclinic, P −1	Monoclinic, P21/n
Temperature (K)	100 K	100 K	100 K	100 K	100 K
a (Å)	7.6114(10)	6.1920(70)	7.5685(12)	7.5868(24)	17.350(30)
b (Å)	10.9778(14)	7.6700(80)	17.9912(27)	18.0066(59)	7.3842(14)
c (Å)	14.6280(20)	27.7130(30)	20.4040(32)	20.8838(71)	20.2780(40)
α(°)	82.325(10)	91.690(38)	72.200(5)	76.406(18)	90
β (°)	84.995(10)	91.550(30)	82.236(6)	88.022(19)	106.010(20)
γ(°)	74.288(8)	104.600(40)	89.356(6)	89.463(17)	90
V ($Å^3$)	1164.38(31)	1272.30(14)	2619.76(51)	2771.41(13)	2497.17(15)
Z	1	1	2	2	2
μ (mm^{-1})	1.416	1.314	1.294	1.239	1.324
Crystal size (mm^3)	0.01, 0.07, 0.08	0.02, 0.08,0.14	0.06, 0.10, 0.27,	0.01, 0.07, 0.18	0.02, 0.09, 0.12
F(000)	546.0	594.0	1284.0	1380.0	1140.0
Data collection					
Diffractometer	Bruker APEX-II CCD area detector diffractometer				
Absorption correction	Based on multi-scan				
No. of measured, independent and observed reflections	35419, 5122, 3693	5343, 4541, 1794	74889, 11912, 8973	40034, 10408, 6356	22546, 3834, 2694
θ_{min} (°)	1.94	2.21	1.82	1.71	1.81
θ_{max} (°)	27.52	29.09	27.50	25.68	23.82
R_{all}, R_{obs}	0.085, 0.044	0.193, 0.064	0.099, 0.070	0.109, 0.049	0.068, 0.036
wR_{2-all}, wR_{2-obs}	0.078,0.069	0.177, 0.130	0.160, 0.148	0.101, 0.084	0.070, 0.064
GOOF	1.036	0.893	1.216	0.984	0.961
No. of parameters	280	316	669	892	299
Δr_{max}, $\Delta\rho_{min}$ (e $Å^{-3}$)	0.712, −1.051	0.177, −0.130	2.252, −1.806	0.716, −0.828	0.462, −0.332
CCDC	1511609	1511611	1511610	1511612	1511613

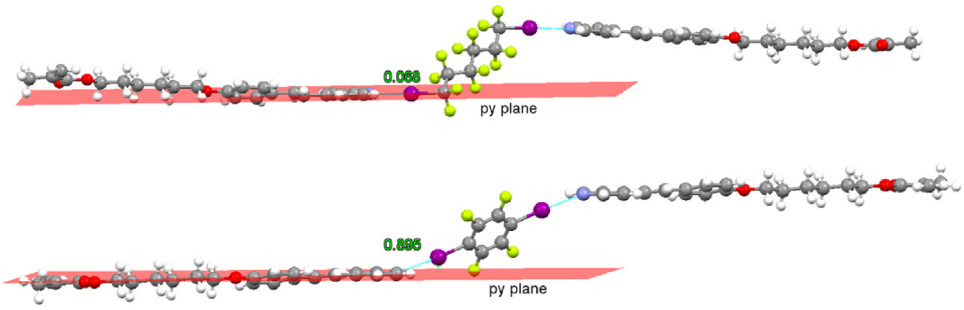

Fig. 1. Ball-and-stick representation of the single crystal X-ray structure of complex **3c** (top) and **3e** (bottom). The stepped organization between the XB donor and acceptor in the supramolecular trimer is shown. The in-plane for **3c** and out-of-plane for **3e** XB are highlighted. The plane described by the pyridyl ring (py plane) is shown in red and the distance between the iodine atom and the plane is reported in Å. Color codes: grey, carbon; blue, nitrogen; magenta, iodine; red, oxygen; yellow, fluorine and white, hydrogen. XB are light blue dotted lines. (For interpretation of the references to colour in this figure legend, the reader is referred to the web version of this article.)

Table 3
Described distances and angles observed in the crystal structure of co-crystals **3a–e**.

Co-crystal	N···I (Å)	N_c[a]	C-I···N (°)
3a	2.829	0.801	175.57
3b	2.934	0.831	173.51
3c	2.773	0.776	176.03
3d	2.759	0.781	178.19
3e	2.824	0.800	174.56

[a] As a measure of the strength of XB, we define 'normalized contact' N_c as the ratio $N_c = D_{ij}/(rvdw_i + rvdw_j)$, where D_{ij} is the distance between the atoms i and j and $rvdw_i$ and $rvdw_j$ are the corresponding van der Waals radii for I and N atoms respectively [38].

Specifically, the co-crystals **3a–d** are characterized by a stepped organization between the two stilbazoles, a direct consequence of the antiperiplanar arrangement of the perfluoromethylene groups of the XB donor (Fig. 1, top and Fig. S1). Similar organization is also observed in the co-crystal **3e**, (Fig. 1, bottom) where the modules **1** adopt a stepped arrangement although the core of the XB-donor is a *para*-substituted aromatic moiety. In this case the effect of the staggered arrangement is promoted by the flexibility of the XB contact. In fact, differently from all other co-crystals where the XBs take place in the plane described by the pyridyl ring of the stilbazole, in **3e** the interaction occurs out-of-plane with a distance between the iodine atom and the projection of the pyridyl ring plane of 0.89 Å. This deviation from the planarity allows for the stepped organization of the stilbazole modules in the trimer (Fig. 1).

Other small differences appear in the arrangement of the donor/acceptor modules in **3a–d**. For instance when the shortest XB donor **2a** is used the CF_2 unit of the chain lays on the same plane described by the pyridyl ring of the stilbazole **1**, while for all the other co-crystals the perfluoroalkyl chains are perpendicular to the plane of the pyridyl rings (Fig. S2).

It is known that perfluorocarbon and hydrocarbon compounds tend to segregate and this phenomenon is directly correlated with the number of fluorine atoms in the fluorinated moieties. This behavior becomes noticeable in the co-crystals **3b–d** where the perfluorinated units form well-defined layers fully separated by the hydrocarbon systems. For instance in **3b** the stilbazoles and the 1,4-diiodoperfluorobutane molecules are stacked in separated columns parallel to the *b* crystallographic axis (Fig. 2, bottom). Differently, when 1,2-diiodotetrafluoroethane **2a** and 1,4-diiodotetrafluorobenzene **2e** are used, the number of fluorine atoms is not enough to elicit the segregation and the XB-donors are surrounded by hydrocarbon units (Fig. 2 top, and Fig. S3). When present, segregation may eventually promote the formation of layered structures, *i.e.* lamellae, also in the molten phase and let us to foresee a liquid crystalline behavior.

Another interesting common structural feature in **3a-d** is that the stilbazoles **1** are stacked in head-to-tail fashion where the alkyl side chain of one stilbazole is sandwiched between the aromatic rings of adjacent stilbazoles and, of course, vice versa (Fig. 2). In **3e** this motif is less pronounced and the stilbazole modules tend to adopt a more distorted packing. This arrangement is a direct consequence of the angle between the two stilbazole units in the trimer.

Finally, the overall crystal packing in all the co-crystals are stabilized by weak C—H···O, H···F, and H···π short contacts

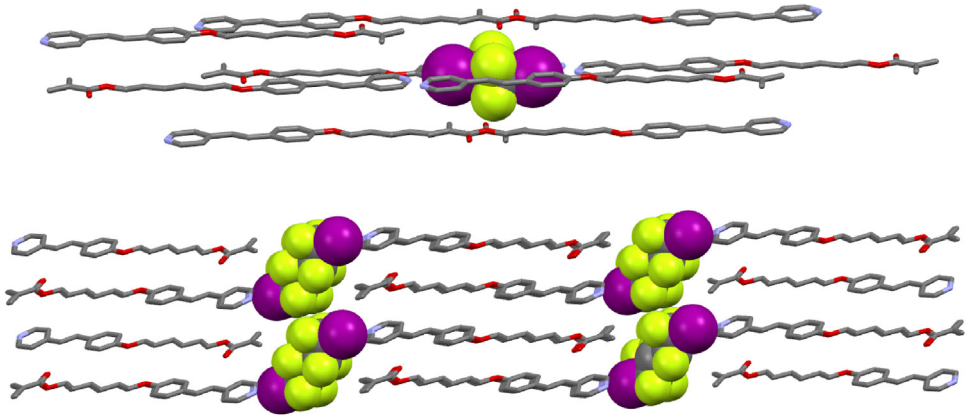

Fig. 2. Crystal packing of complexes **3a** (top) and **3b** (bottom) showing a clear segregation between hydrocarbon and perfluorocarbon modules in complex **3b**. Hydrogen atoms have been omitted for the sake of clarity. Color codes: grey, carbon; blue, nitrogen; magenta, iodine; red, oxygen; yellow, fluorine. (For interpretation of the references to colour in this figure legend, the reader is referred to the web version of this article.)

Table 4
Thermal behavior of complexes **3a–e** from POM analysis.

Co-crystal	Melting point (°C)		Phase transition	T/°C
	XB-Acceptor (1)	XB-Donor (2)		
3a	78	−21	Cr—I	95
3b	78	−9	Cr—I	106
			I—Sm A	80
			(Sm A—I)	97
			Sm—Cr	52
3c	78	25	Cr—I	98
			I—Sm A	82
			(Sm A—I)	94
			Sm—Cr	74
3d	78	75	Cr—I	103
			I—Sm A	81
			(Sm A—I)	95
			Sm A—Cr	65
3e	78	110	Cr—I	113
			I—Sm A	92
			(Sm A—I)	104
			Sm A—Cr	78

occurring between adjacent stilbazoles and close perfluorinated compounds.

2.4. Thermal analysis

The liquid crystalline properties of complexes **3a–e** were examined by hot stage polarized optical microscopy (POM). All the starting materials are non mesomorphic and their melting points are reported in Table 4. On heating all the XB-complexes **3a–3e** melted directly to an isotropic liquid although at temperatures higher than the pure XB-donor and acceptors. This gives a further reliable proof that **3a–3e** are well-defined new chemical species rather than a mechanical mixture of starting modules. Moreover, these data prove that a simple one-pot co-crystallization procedure can be easily exploited to stabilize volatile perfluorinated compounds, since the occurrence of halogen bond remarkable decreases their volatility [39].

This is remarkable taking into account the high volatility of haloperfluoroalkanes and the increasing concerns regarding their potential role as persistent and bioaccumulative organic pollutants.

On cooling from the isotropic liquid, a monotropic SmA phase appeared for complexes **3b-e**, (Fig. 3, Fig. S5 and Table 4 while complex **3a** decomposed soon after melting. This is because of the higher volatility of the diiodoperfluoroethane module, which upon heating evaporated from the liquid mixture. The mesogenic behavior found for **3b-e** is perfectly reproducible even after several excursions in the isotropic phase, and smectic A phases were observed over a range of 20–30 °C before the material crystalized, except for **3b** whose LC phase appeared longer lived and reproducibly existed for some 45 °C before crystallization occurred.

This suggests that the XB interaction survives in the liquid crystalline phase and has an appreciable strength, similar to that seen in previously reported hydrogen-bonded systems [40]. The observation of a SmA phase is consistent with XRD analysis and is a manifestation of nanofase segregation of perfluorocarbons and hydrocarbons modules.

The reported data show that despite the non-mesomorphic nature of the starting materials, most of the halogen-bonded complexes show liquid-crystalline behavior, further confirming the effectiveness of the XB in the construction of new supramolecular mesogens.

3. Conclusions

In summary, we have described the synthesis of new trimeric complexes obtained upon XB-driven self-assembly of 1,4-diiodotetrafluorobenzene or α,ω–diiodoperfluoroalkanes, acting as XB-donors, with an alkoxystilbazole derivative functionalized with a methacrylate terminal group, acting as XB-acceptor. Despite the non-mesomorphic nature of the starting materials, most of the halogen-bonded complexes show liquid-crystalline behavior with smectic A phases. Single crystal X-ray diffraction analysis confirmed that N···I XB interactions are largely responsible for the self-assembly of the complementary modules **1** and **2** and showed a clear segregation between perfluorocarbon and hydrocarbon molecules that perfectly agree with the lamellar phase observed in the LC state.

All the reported complexes decompose at temperatures higher than the melting points of the starting diiodoperfluorocarbons proving that an XB-driven cocrystallization can be exploited as an easy and convenient tool to stabilize volatile perfluorinated compounds.

The obtained supramolecular mesogens possess reactive groups suitable for incorporation into liquid crystalline elastomeric actuators.

4. Experimental

4.1. Materials and methods

Commercial HPLC-grade solvents were used without further purification. Starting materials were purchased from Sigma–Aldrich, Acros Organics, and Apollo Scientific. IR spectra were obtained using a Nicolet Nexus FT-IR spectrometer equipped with

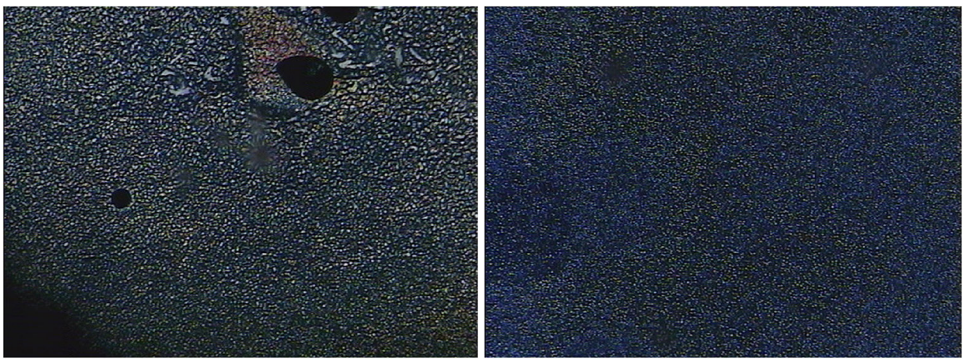

Fig. 3. Optical textures of the smectic A phase observed on cooling from the isotropic state for complex **3d** (left; T = 81 °C) complex **3e** (right; T = 92 °C).

UATR unit (4000–400 cm^{-1} range). Differential scanning calorimetry (DSC) analysis were performed on a Mettler Toledo DSC823e instrument using aluminum light 20 μL sample pans and the Mettler: STARe software for calculation of thermal behavior. The LC textures were studied with an Olympus BX51 polarized optical microscope equipped with a Linkam Scientific LTS 350 heating stage and a Sony CCD-IRIS/RGB video camera.

4.2. Synthesis of 6-(pyridin-4-yloxy)hexyl methacrylate (*1*)

The synthesis of the stilbazole methacrylate has been carried out according the literature [41].

mp 78–80 °C; ^{1}H NMR (400 MHz, $CDCl_3$) δ: 1.50 (m, 4H, CH_2), 1.72 (q, 2H, *J* = 14.0 Hz, CH_2), 1.82 (q, 2H, *J* = 13.8 Hz, CH_2), 1.95 (s, 3H, CH_3), 3.99 (t, 2H, *J* = 6.5 Hz, $ArOCH_2$), 4.15 (t, 2H, *J* = 6.5 Hz, OCH_2), 5.55 (m, 1H, C=H), 6.10 (m, 1H, C=H) 6.87 (d, 1H, *J* = 15.4 Hz, CH) 6.90 (d, 2H, *J* = 8.7 Hz, phenyl-H), 7.25 (d, 1H, *J* = 16.3 Hz, CH), 7,33 (d, 2H, *J* = 6.1 Hz, pyridyl-H), 7.47 (d, 2H, *J* = 8.7 Hz, phenyl-H), 8.55 (d. 2H, *J* = 6.1 Hz, pyridyl-H). ^{13}C NMR (400 MHz, $CDCl_3$) δ: 167.6, 159.7, 150.3, 150.1, 145.0, 136.6, 132.9, 128.8, 128.5, 128.3, 125.4, 125.2, 120.8, 120.5, 114.9, 114.8, 67.9, 64.7, 29.2, 28.6, 25.9, 25.8; FTIR (cm^{-1}): 3071, 3036, 2943, 2899, 2886, 1701, 1594, 1514, 1169, 1023, 873, 545; MS *m/z*. 366.13 (M+H+) (calculated for $C_{23}H_{27}NO_3$, 365.20).

4.3. Crystallization of co-crystals *3a–e*

Two equivalents of stilbazole methacrylate and one equivalent of 1,4-diiodoperfluorocarbons were dissolved in THF at room temperature in a clear borosilicate glass vial. The open vial was placed in a closed cylindrical wide-mouth bottle containing paraffin. The THF was allowed to diffuse at room temperature.

Co-crystal 3a. Yellowish needle shaped crystals; mp 95 °C; FTIR (cm^{-1}): **1, 2-diiodotetrafluoroethane (2a):** 1206, 1146, 1096, 972, 833, 685, 574; **Complex 3a:** 3073, 3040, 2935, 2907, 1590, 1511, 1196, 1123, 1087, 1014, 962, 826, 700, 545.

Co-crystal 3b. Yellowish needle shaped crystals; mp 106 °C; FTIR (cm^{-1}): **1, 4-diiodooctafluorobutane (2b):** 1189, 1130, 1085, 1039, 977, 887, 834, 634, 555; **Complex 3b:** 3072, 3040, 3053, 2899, 2884, 1173, 1122, 1064, 1020, 954, 831, 760, 548.

Co-crystal 3c. Yellowish needle shaped crystals; mp 98 °C; IR (cm^{-1}): **1, 6-diiodododecafluorohexane (2c):** 1210, 1141, 1084, 925, 833, 789, 730, 634, 552; **Complex 3c:** 2955, 2878, 1174, 1113, 1061, 1016, 925, 833, 732, 549.

Co-crystal 3d. Yellowish needle shaped crystals; mp 103 °C; IR (cm^{-1}): **1, 8-diiodohexadecafluorooctane (2d):** 1207, 1146, 1055, 959, 838, 631, 561; **Complex 3d:** 3074, 3037, 2945, 2822, 1175, 1102, 1060, 1015, 955, 832, 545.

Co-crystal 3e. Yellowish block shaped crystals; mp 113 °C; IR (cm^{-1}): **1, 4-diiodotetrafluorobenzene (2e):** 1459, 1362, 1210, 969, 940, 757, 561; **Complex 3e:** 3096, 3044, 2906, 2894, 1707, 1511, 1456, 1196, 1123, 1087, 1014, 936, 540.

4.4. Analysis by X-ray diffraction

Single crystal X-ray data were collected on a Bruker KAPPA APEX II Diffractometer with Mo-Kα radiation (λ = 0.71073) and CCD detector. To reduce the possibility of phase transition at all data sets was collected at low temperature (90 K) using Bruker KRYOFLEX device. The structures were solved by SIR2002 [42] and refined by SHELXL-97 [43] programs, respectively. The refinement was carried on by full-matrix least-squares on F^2. Hydrogen atoms were placed using standard geometric models and with their thermal parameters riding on those of their parent atoms. Diiodoperfluorooctane in complex **1d** was disordered in two opposite helical, nearly *all-trans* conformations, with great separation of fluorine atoms, so that the whole molecules could be split and refined with few restraints on the perfluorocarbon geometry.

Acknowledgments

P.M. acknowledges the European Research Council (ERC) for funding the Starting Grant ERC-2012-StG_20111012 FOLDHALO (Grant Agreement Number 307108).

Appendix A. Supplementary data

Supplementary data associated with this article can be found, in the online version, at http://dx.doi.org/10.1016/j.jfluchem.2016.12.011.

References

[1] H.K. Bisoyi, S. Kumar, Chem. Soc. Rev. 40 (2011) 306–319.
[2] M. Bremer, P. Kirsch, M. Klasen-Memmer, K. Tarumi, Angew. Chem. – Int. Ed. 52 (2013) 8880–8896.
[3] J.P.F. Lagerwall, G. Scalia, Curr. Appl. Phys. 12 (2012) 1387–1412.
[4] G. Fernández, Nat. Mater. 12 (2012) 12–14.
[5] D. Iqbal, M.H. Samiullah, Materials (Basel) 6 (2013) 116–142.
[6] H. Thiem, P. Strohriegl, M. Shkunov, I. McCulloch, Macromol. Chem. Phys. 206 (2005) 2153–2159.
[7] G.M. Bögels, H.P.C. van Kuringen, I.K. Shishmanova, I.K. Voets, A.P.H.J. Schenning, R.P. Sijbesma, Adv. Mater. Interfaces 2 (2015) 1500022.
[8] S.J. Lee, J.Y. Jho, J.H. Lee, Mol. Cryst. Liq. Cryst. 621 (2015) 175–181.
[9] B.U. Theissen, S.J. Zilker, T. Pfeuffer, P. Strohriegl, Adv. Mater. 12 (2000) 1698–1700.
[10] L.T. De Haan, J.M.N. Verjans, D.J. Broer, C.W.M. Bastiaansen, A.P.H.J. Schenning, J. Am. Chem. Soc. 136 (2014) 10585–10588.
[11] S. Petsch, B. Khatri, S. Schuhladen, L. Köbele, R. Rix, R. Zentel, H. Zappe, Smart Mater. Struct. 25 (2016) 85010.
[12] D.J. Mulder, A.P.H.J. Schenning, C.W.M. Bastiaansen, J. Mater. Chem. C 2 (2014) 6695–6705.
[13] J. Mamiya, Polym. J. 45 (2012) 239–246.
[14] A. Priimagi, G. Cavallo, P. Metrangolo, G. Resnati, Acc. Chem. Res. 46 (2013) 2686–2695.
[15] G.R. Desiraju, P.S. Ho, L. Kloo, A.C. Legon, R. Marquardt, P. Metrangolo, P. Politzer, G. Resnati, K. Rissanen, Pure Appl. Chem. 85 (2013) 1711–1713.
[16] P. Politzer, J.S. Murray, T. Clark, Phys. Chem. Chem. Phys. 12 (2010) 7748–7757.
[17] C.B. Aakeröy, P.D. Chopade, J. Desper, Cryst. Growth Des. 13 (2013) 4145–4150.
[18] K.E. Riley, J.S. Murray, J. Fanfrlík, J. Řezáč, R.J. Solá, M.C. Concha, F.M. Ramos, P. Politzer, J. Mol. Model. 17 (2011) 3309–3318.
[19] L.J. McAllister, C. Präsang, J.P.-W. Wong, R.J. Thatcher, A.C. Whitwood, B. Donnio, P. O'Brien, P.B. Karadakov, D.W. Bruce, Chem. Commun. (Camb.) 49 (2013) 3946–3948.
[20] D.W. Bruce, Halogen Bond, in: P. Metrangolo, G. Resnati (Eds.), Fundam. Appl., Springer-Verlag, Berlin Heidelberg, 2008, pp. 161–180.
[21] D.W. Bruce, P. Metrangolo, F. Meyer, T. Pilati, C. Praesang, G. Resnati, G. Terraneo, S.G. Wainwright, A.C. Whitwood, Chem. – A Eur. J. 16 (2010) 9511–9524.
[22] G. Cavallo, P. Metrangolo, R. Milani, T. Pilati, A. Priimägi, G. Resnati, G. Terraneo, Chem. Rev. 116 (2016) 2478–2601.
[23] P. Metrangolo, C. Präsang, G. Resnati, R. Liantonio, A.C. Whitwood, D.W. Bruce, Chem. Commun. (Camb.) (2006) 3290–3292.
[24] M. Hird, Chem. Soc. Rev. 36 (2007) 2070–2095.
[25] P. Kirsch, J. Fluor. Chem. 177 (2015) 29–36.
[26] A. Abate, A. Petrozza, G. Cavallo, G. Lanzani, F. Matteucci, D.W. Bruce, N. Houbenov, P. Metrangolo, G. Resnati, J. Mater. Chem. A Mater. Energy Sustain. 1 (2013) 6572–6578.
[27] A. Abate, A. Petrozza, V. Roiati, S. Guarnera, H. Snaith, F. Matteucci, G. Lanzani, P. Metrangolo, G. Resnati, Org. Electron. 13 (2012) 2474–2478.
[28] D.W. Bruce, P. Metrangolo, F. Meyer, C. Prasang, G. Resnati, G. Terraneo, A.C. Whitwood, C. Praesang, G. Resnati, G. Terraneo, A.C. Whitwood, N. J. Chem. 32 (2008) 477–482.
[29] J. Xu, X. Liu, T. Lin, J. Huang, C. He, Macromolecules 38 (2005) 3554–3557.
[30] A. Priimagi, M. Saccone, G. Cavallo, A. Shishido, T. Pilati, P. Metrangolo, G. Resnati, Adv. Mater. (Weinheim Ger.) 24 (2012) OP345–OP352.
[31] C.B. Aakeröy, S. Panikkattu, P.D. Chopade, J. Desper, CrystEngComm 15 (2013) 3125–3136.
[32] A. Abate, S. Biella, G. Cavallo, F. Meyer, H. Neukirch, P. Metrangolo, T. Pilati, G. Resnati, G. Terraneo, J. Fluor. Chem. 130 (2009) 1171–1177.
[33] M. Baldrighi, P. Metrangolo, F. Meyer, T. Pilati, D. Proserpio, G. Resnati, G. Terraneo, J. Fluor. Chem. 131 (2010) 1218–1224.
[34] L. Catalano, P. Metrangolo, T. Pilati, G. Resnati, G. Terraneo, M. Ursini, J. Fluor. Chem. (2016).

[35] K. Willis, D.J. Price, H. Adams, G. Ungar, D.W. Bruce, J. Mater. Chem. 5 (1995) 2195–2199.
[36] B. Hawthorne, H. Fan-Hagenstein, E. Wood, J. Smith, T. Hanks, Int. J. Spectrosc. (2013) 1–10.
[37] Q.J. Shen, W.J. Jin, Phys. Chem. Chem. Phys. 13 (2011) 13721–13729.
[38] A. Bondi, J. Phys. Chem. 68 (1964) 441–451.
[39] C.B. Aakeröy, T.K. Wijethunga, J. Desper, C. Moore, J. Chem. Crystallogr. 45 (2015) 267–276.
[40] H.L. Nguyen, P.N. Horton, M.B. Hursthouse, A.C. Legon, D.W. Bruce, J. Am. Chem. Soc. 126 (2004) 16–17.
[41] H.C. Lin, J. Hendrianto, Polymer (Guildf) 46 (2005) 12146–12157.
[42] M.C. Burla, B. Camalli, Mercedes Carrozzini, G.L. Cascarano, C. Giacovazzo, G. Polidoria, R. Spagnabzini, J. Appl. Crystallogr. 36 (2003) 1103.
[43] G.M. Sheldrick, Acta Crystallogr. Sect. C Struct. Chem. 71 (2015) 3–8.